Innovative Food Science and Emerging Technologies 74 (2021) 102872

Contents lists available at ScienceDirect

Innovative Food Science and Emerging Technologies

journal homepage: www.elsevier.com/locate/ifset

PEF-treated plant and animal tissues: Insights by approaching with different electroporation assessment methods

Jessica Genovese [a], Matej Kranjc [b], Igor Serša [c], Massimiliano Petracci [a], Pietro Rocculi [a], Damijan Miklavčič [b], Samo Mahnič-Kalamiza [b,*]

[a] University of Bologna, Alma Mater Studiorum, Department of Agricultural and Food Sciences, P. Goidanich 60, Cesena, Italy
[b] University of Ljubljana, Faculty of Electrical Engineering, Tržaška c. 25, 1000 Ljubljana, Slovenia
[c] Institut "Jožef Stefan", Jamova c. 39, 1000 Ljubljana, Slovenia

ARTICLE INFO

Keywords:
PEF treatment
Electrical impedance spectroscopy
Electric current analysis
Tissue conductivity
Magnetic resonance imaging

ABSTRACT

The goal of our investigation was to explore the level of membrane permeabilization in plant and animal food matrices (potato, apple, chicken) as resulting from subjecting these matrices to pulsed electric field treatment whereby we employed different assessment methods (electrical impedance spectroscopy, current-voltage measurements, magnetic resonance imaging). Our study was performed using a number of amplitudes of eight electric pulses of 100 μs in duration, and results were expressed in terms of the change in electrical properties as evaluated by electrical impedance spectroscopy, current-voltage measurements, and changes in the water (re) distribution as evaluated by magnetic resonance imaging and T_2 mapping techniques. The findings of our research provide useful insights and could be in support of an appropriate choice of electroporation assessment methods in relation to the food matrix characteristics, and for the determination and selection of appropriate PEF treatment conditions.

1. Introduction

Electroporation or pulsed electric field (PEF) treatment is a process known to cause an increase of cell membrane permeability and consequently an increase of the cell membrane and tissue conductivity. This phenomenon takes place when a biological tissue is exposed to an externally applied electric field of sufficient strength and is most often explained by the creation of aqueous pathways (i.e. pores) in the lipid domain of the cell membrane (Kotnik, Rems, Tarek, & Miklavcic, 2019). The application of PEF treatment in food processing is gaining momentum, and it is currently under intensive research and development. New electroporation-based treatments are continuously put to the test and are optimized both at the laboratory and industrial scale processes (Mahnič-Kalamiza, Vorobiev, & Miklavčič, 2014). PEF treatment offers increasing benefits in terms of low energy requirements and minimization of food quality deterioration. Following this preamble, it becomes clear that an appropriate choice of methods assessing changes due to electroporation occurring in biological matrices of alimentary interest is crucial. Despite a considerable number of scientific papers accumulated in the field, detailed information regarding the detection and quantification of the effects of electroporation in complex and highly inhomogeneous multicellular systems, such as real food systems, is still limited. Moreover, due to the unique characteristics and properties of the biological tissue processed, a case-by-case PEF treatment optimization protocol is often required (Bhat, Morton, Mason, & Bekhit, 2019; Chalermchat, Malangone, & Dejmek, 2010; Golberg et al., 2016).

In food-related PEF applications, measurements of the dielectric properties of the tissue are often used for the determination of the degree of cell membrane disruption due to electroporation (Lebovka & Vorobiev, 2017). The electrical impedance spectroscopy (EIS) has been suggested as a reliable method to estimate the extent of tissue damage due to PEF treatment. This method relies on the theory that, from an electrical point of view, an individual cell can be represented as an insulating membrane exhibiting relatively high resistance to electric current and considerable capacitance, and intra- and extra-cellular media (electrolytes) that behave as a resistive (ohmic) load up to hundreds of MHz (Grimnes, Martinsen, Grimnes, & Martinsen, 2015). Most animal and vegetable tissues typically display a dispersion of impedance between low- and high-frequency fields, that arise at a spectral band starting from about 50 Hz and ending at about 10 MHz (Castellví,

* Corresponding author.
E-mail address: Samo.Mahnic-Kalamiza@fe.uni-lj.si (S. Mahnič-Kalamiza).

https://doi.org/10.1016/j.ifset.2021.102872
Received 3 September 2021; Received in revised form 10 November 2021; Accepted 11 November 2021
Available online 14 November 2021

Mercadal, & Ivorra, 2017). Multifrequency impedance measurement can therefore be used to assess the degree of membrane permeabilization due to PEF treatment (Angersbach, Heinz, & Knorr, 2002), and its utility has already been demonstrated for various biological systems (Angersbach, Heinz, & Knorr, 1999; Cukjati, Batiuskaite, André, Miklavčič, & Mir, 2007; Mahnič-Kalamiza, Miklavčič, & Vorobiev, 2015). Another possible but infrequently used approach for the evaluation of tissue electrical properties involves the analysis of the voltage and current waveforms recorded during the application of the electric pulses. Electric current signals can be used to detect changes in the dielectric properties of the cell membrane in real-time, and can thus be used to assess the electroporation process. A discrete number of research papers reported the analysis of the current signals during the application of the high-voltage pulse, and it has been demonstrated that the dynamics of current can be used as a key characterization feature of tissue electroporation (Cukjati et al., 2007; Langus, Kranjc, Kos, Šuštar, & Miklavčič, 2016; Lv et al., 2020; Pavlin & Miklavčič, 2008).

Nevertheless, measuring changes in the electrical properties, such as complex impedance for example, presents a clear drawback of being affected by additional (accounted or unaccounted for) phenomena, whose effects may be mixed with (or superimposed to) physical changes of interest that take place after exposure to PEF. Biological tissues present high complexity of structure and spatially dependent properties, and it has been demonstrated that the modification of cell membrane permeabilization due to electroporation is also associated with modification of the structure (i.e. intra- and extracellular volume change), and ionic concentration variation due to leakage of intracellular content (Mahnič-Kalamiza et al., 2015; Pavlin et al., 2005). Hence, other techniques evaluating the effects of tissue electroporation have been suggested. Magnetic resonance imaging (MRI) techniques have been applied to monitor the spatially dependent effect of PEF treatment in vegetable tissues (Dellarosa et al., 2018; Kranjc, Bajd, Serša, de Boevere, & Miklavčič, 2016). Transverse relaxation time T_2 has been employed as an indication of the redistribution of water and solutes in the tissue following the PEF treatment (Hjouj & Rubinsky, 2010). Moreover, MRI and magnetic resonance electrical impedance tomography (MREIT) were proposed as methods to monitor the electric field distribution in the tissue while applying the PEF treatment (Kranjc et al., 2016).

In our study we combined the electrical impedance spectroscopy, the current-voltage measurements, and the magnetic resonance imaging technique to explore the level of membrane permeabilization occurring due to electroporation in raw plants and skeletal muscles of interest for food and/or feed. We examined the variation of electrical properties and water mobility of vegetable and animal tissues subjected to various intensities of PEF treatment in order to investigate the consistency of the PEF assessing methods in relation to the type of food matrix. Experiments were performed in potato tuber and apple tissue since these vegetable matrices are of high interest in industrial PEF applications. Chicken broiler *Pectoralis major* was selected as a reference skeletal muscle, as it is one of the most homogeneous muscles in farmed animals, being almost entirely constituted of IIB fibre type, i.e. fast-twitch glycolytic (Verdiglione & Cassandro, 2013). We performed impedance measurements before and after the application of pulses, as it is an often used method in food-related PEF applications to determine the degree of membrane disruption (Lebovka & Vorobiev, 2017). We also performed and analysed current and voltage measurements to gain additional information about the electroporation of cell membranes, as well as magnetic resonance imaging for the characterization of the tissue's PEF-response by T_2 mapping.

2. Materials and methods

2.1. Raw materials

2.1.1. Plant tissues

Two different plant tissues were used for this study: potato tubers (*Solanum tuberosum*, cv 'Liberta'), and apples (*Malus domestica*, cv 'Golden Delicious'), purchased from the local market. At the time of experiments, the soluble solid content of apples was 11.3 ± 0.3°Brix.

The raw materials, before trials, were manually cut using a sharp cork-borer to obtain cylindrical-shape samples of 26 mm in diameter. The thickness of the disks was 6 mm for electrical impedance spectroscopy, and 30 mm for magnetic resonance imaging.

2.1.2. Skeletal muscle tissues

Boneless and skinless *Pectoralis major* muscles were obtained from the same flock of broiler chickens (Ross 308 hybrid, slaughter age 46 days, average weight 2.9 kg) farmed and processed under commercial conditions and, before trials, stored at 1 °C. Trials were conducted 48 h *post-mortem*. Each fillet was sampled using the cranial portion of the breast and cut along the direction of muscle fibres. From each sample, disks of 26 mm in diameter were manually cut using a sharp cork-borer. The thickness of the disks was 6 mm for electrical impedance spectroscopy, and 30 mm for magnetic resonance imaging.

2.2. Experimental setup

2.2.1. Electrical impedance spectroscopy and current-voltage measurements

Two electrical impedance measurement systems were assembled by connecting: 1) 4-needle electrodes, and 2) a treatment chamber consisting of two stainless-steel parallel plate electrodes, to a precision LCR meter (model E4980A, Keysight Inc., USA). The needle electrodes (copper with nickel plating) were 6 mm long and 1 mm in diameter and were spaced 5 mm (centre-to-centre) from each other along a straight line. All four electrodes were employed to deliver the high-voltage electroporation pulses, with the left-most two electrodes connected (in parallel) to one polarity on the generator, and the right-most two electrodes connected (in parallel) to the opposite polarity. In the case of two-plate electrodes, the treatment chamber was used to hold the sample, while the electrodes, spaced at 6 mm from each other, were employed to both deliver the high-voltage electroporation pulses as well as for impedance measurements. In both systems, switching relays were used to switch the electrical connections of the electrodes between the high-voltage pulse generator and the LCR meter.

Cylindrical samples were treated by delivering 8 rectangular monopolar pulses of 100 μs duration to the tissue with a pulse repetition rate of 1 Hz. For each treatment, different pulse amplitudes were used; from 50 V to 1500 V for plant tissues, and from 250 V to 1500 V for animal tissues.

Multi-frequency parallel capacitance (C_p) and parallel resistance (R_p) measurements of untreated and treated samples (i.e. between 3 and 5 s after the pulse application) were performed in the frequency range of 50 Hz to 1 MHz by applying a 100 mV (for plant tissues) and 500 mV (for animal tissues, due to the higher conductivity compared to plant tissues) peak voltage to the outer electrodes. The outer electrodes (centre-to-centre distance 15 mm) thus served as the current source and sink, while the inner pair (centre-to-centre distance 5 mm) were used to measure the voltage drop, as customarily configured in 4-electrode impedance analysis. Data were acquired using an in-house developed software for the LCR meter control and data capture (based on the Arduino and National Instruments LabVIEW software platforms). The magnitude of impedance was calculated according to Eq. (1).

$$|Z| = \left(\sqrt{\left(\frac{1}{R_p}\right)^2 + \left(\omega C_p\right)^2} \right)^{-1} \quad (1)$$

where R_p and C_p are the measured resistance and capacitance in parallel, respectively, and ω is the angular frequency ($\omega = 2\pi f$) and f is the excitation signal frequency in range of 50 Hz to 1 MHz as set in the impedance analyser.

For each PEF treatment, the delivered voltage and current were

measured and recorded by a high-voltage probe (model HVD3206A, LeCroy USA) and a current probe (model CP031A, LeCroy USA) connected to a sequencing digital storage oscilloscope (model HDO6104A-MS, LeCroy USA). The recorded voltage-current data were analysed using MATLAB 2019b software (MathWorks, Natick, MA, USA).

2.2.2. Magnetic resonance imaging (MRI)

Magnetic resonance imaging (MRI) was performed on plant and animal tissues while applying the PEF treatment. PEF treatment protocol consisted of two sequences of 4 pulses of 100 μs duration, with a pulse repetition frequency of 5 kHz and adjusting the voltage amplitude to obtain sufficient signal-to-noise ratio of electric field in samples. The electric pulses were delivered using a laboratory prototype electric pulse generator (Novickij et al., 2016) connected to 2-needle electrodes with a diameter of 1 mm made of platinum-iridium alloy (Pt/Ir: 90/10%). Electrodes were inserted into the sample tissue at a centre-to-centre distance of 10.4 mm, and the samples were PEF-treated while they were scanned by the MRI. The MRI scanner consisted of a 2.35 T (100 MHz proton nuclear MR frequency) horizontal bore superconducting magnet (Oxford Instruments, Abingdon, UK) connected to an Apollo spectrometer (Tecmag, Houston TX, USA) and equipped with micro-imaging accessories with maximum gradients of 250 mT/m (Bruker, Ettlingen, Germany).

2.2.2.1. Current density imaging (CDI) and magnetic resonance electrical impedance tomography (MREIT). The Current Density Imaging (CDI) method relies on current-induced magnetic field change in the sample that is detected via phase shift registration by magnetic resonance imaging (Joy, Scott, & Henkelman, 1989). Next, Magnetic Resonance Electrical Impedance Tomography (MREIT) J-substitution algorithm, based on iterative solving of the Laplace equation, was employed to calculate the conductivity map and also the electric field by using CDI data along with known sample geometry and potentials on the electrodes as inputs for the algorithm (Khang et al., 2002; Kranjc et al., 2016).

The two-shot RARE CDI pulse sequence (Serša, 2008) was used to image current density in the biological tissues during application of electric pulses. Delivery of electroporation pulses was synchronized with the CDI sequence using TTL pulses from the NMR/MRI spectrometer to trigger the electric pulse generator. The following imaging parameters were used: field of view 30 mm; imaging matrix 64 × 64; inter-echo delay 2.64 ms. In the sequence, block of electroporation pulses was positioned between the excitation RF pulse and the first refocusing RF pulse. MREIT was performed by using the finite element method with the numerical computational environment MATLAB 2019b (MathWorks, Natick, MA, USA) on a desktop personal computer.

2.2.2.2. Multiparametric magnetic resonance imaging (MRI). A multi-spin-echo (MSE) imaging sequence based on the Carr-Purcell-Meiboom-Gill (CPMG) multi-echo train (Carr & Purcell, 1954) was chosen to acquire T_2 weighted MR images. T_2 mapping was performed before and immediately after the PEF treatment (i.e. total imaging time 18 min after the PEF treatment). The calculation of T_2 maps was performed by the MRI Analysis Calculator plug-in of the ImageJ (NIH; US) image-processing software, fitting raw MSME data at variable TE (n = 8 echoes) ($R^2 > 0.9$).

2.3. Statistical analysis

Significant differences among the results were evaluated by paired samples Student's *t*-test, parametric analysis of variance (ANOVA) and Tukey multiple comparison, with a significance level of 95% ($p < 0.05$). If Shapiro-Wilk test for normality and Levene's test for homoscedasticity of data resulted statistically significant ($p < 0.05$), non-parametric multiple range test Kruskal-Wallis and Holm stepwise adjustment were used, with significant level of 95% ($p < 0.05$) (R Foundation for Statistical Computing, Austria). Results are expressed as mean ± standard deviations of replications (n = 4).

3. Results

3.1. Impedance measurements

For various applied voltage amplitudes and different materials analysed, the ratio between the absolute impedance value after the electroporation ($|Z_2|$) and before PEF treatment ($|Z_1|$) is reported. As a result of β dispersion (i.e. the phenomenon associated with the polarization of the cell membrane), the frequency dependence of the impedance can be observed in plant tissues (Figs. 1, 2 A,C). Considering that low-frequency currents cannot penetrate the intact cell membrane and are restricted to pass via the extracellular space; when electroporation occurs, it will cause an increase of cell membrane permeability, resulting in a decrease in the magnitude of electrical impedance (i.e. low-frequency currents can pass through the intracellular space). Hence, for a better visualization of the dependency of the impedance decrease on the magnitude of the applied electric field, the normalized absolute impedance at sampling frequency of 5 kHz is shown (Figs. 1, 2 B,D). The indicated frequency has been selected considering that, in the case of two-electrode impedance measurements, the method suffers from electrode polarization effects. Thus, a high enough frequency must be used to enable comparison of plate to 4-electrode measurements. Moreover, for both electrodes configurations (4-needle and plate electrodes) it has to be taken into account that the impedance value (Z_2) depends on the pulse parameters applied (i.e. 8 pulses of 100 μs in duration).

In the potato tissue, a consistent drop of the normalized impedance from approx. 1 (i.e. no differences in the impedance measured after electroporation compared to the corresponding value before electroporation) to 0.57 ± 0.07, measured with 4-needle electrodes, has been attained after applying 150 V (Fig. 1B). The same critical electroporation value was found when parallel-plate electrodes (i.e. two-electrode measurements) were used (Fig. 1D), showing a significant drop of the impedance magnitude at 150 V of applied voltage amplitude (i.e. electric field strength of 250 V/cm, calculated as the ratio between the applied voltage and the electrodes distance). For both methods used, i.e. needles and plates, applied voltage amplitudes above 500 V did not result in a further impedance decrease, suggesting that maximum cell membrane permeabilization was achieved using this particular experimental protocol (i.e. number of pulses and pulse duration) (Fig. 1 B,D). Given the similar inter-electrode distance between the two electrode configurations (i.e. 6 mm for plates and 5 mm for needles), the same absolute voltages result in comparable voltage-to-distance ratios, thus in comparable electric field strength (although it is important to remember that the field strength is highly inhomogeneous for needle electrodes).

Apple tissue showed a pronounced and significant decrease ($p < 0.05$) in the normalized impedance when 300 V pulses were applied with 4-needle electrodes (Fig. 2B), as well as when applied with parallel-plate electrodes (U = 300 V, i.e. 500 V/cm voltage-to-distance ratio) (Fig. 2D).

We also used the 4-needle electrodes configuration system to evaluate the anisotropy of skeletal muscles at different levels of PEF (i.e. how impedance varies when electric field vector is aligned predominantly along or across muscle fibres). Results of the absolute impedance ratio with both fibre orientations, parallel (along the fibres) and perpendicular (across the fibres), are reported (Fig. 3B). As opposed to the needle electrode configuration, with plate electrodes the electric field was applied only perpendicularly to the muscle fibre orientation. The absolute impedance ratio for chicken breast showed much smaller differences, compared to plant tissues, when plotted on the same scale as in Figs. 1,2. However, on an expanded scale, the ratio decreases with the amplitude of the applied voltage (Fig. 3 B,D – see inserts). The decrease of the normalized impedance started to be significant ($p < 0.05$) after

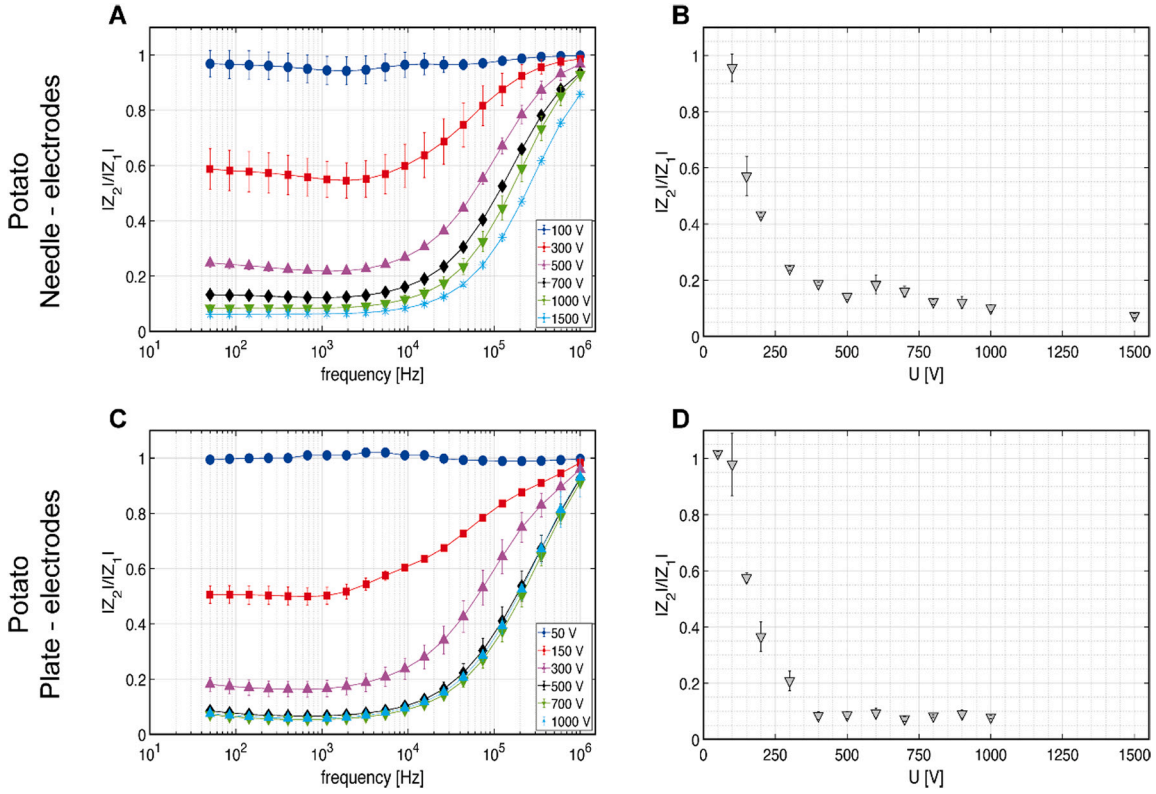

Fig. 1. Potato tuber normalized absolute impedance versus frequency at different applied voltage [U] amplitudes measured with 4-needle-electrodes (A), and plate-electrodes (C) configuration (not all the applied voltages are shown for clarity of presentation). Normalized absolute impedance at sampling frequency of 5 kHz versus the applied voltage [U] measured with 4-needle-electrodes (B), and plate-electrodes (D) configuration. Results are expressed as means ± standard deviations (error bars) of n = 4.

applying a voltage of amplitude of 1200 V, for both needle- and plate-electrodes (Fig. 3 B,D). As shown in Fig. 3B, the electrical impedance spectroscopy did not show any skeletal muscle tissue anisotropy, as the variations of the normalized absolute impedance did not present any statistical difference ($p > 0.05$) between the parallel and the perpendicular orientation of the muscle fibres.

3.2. Voltage-current signal analysis

The changes of the dielectric properties of tissues occurring due to electroporation can also be assessed by analysing the current during the application of electric pulses. Electric current signals can be used to detect changes in the dielectric properties of the cell membrane, and it can thus be used to assess the electroporation process. A typical current signal during PEF application to a tissue consist of a rapid initial increase followed by an exponential decrease (a current spike), which corresponds to the current required for charging of the membrane. When electroporation occurs, the current shows further increase before reaching a constant level at the end of the pulse (schematic presentation in Fig. 4A). This further increase during the pulse is consistent with the cell membrane permeabilization (Cukjati et al., 2007; Pavlin & Miklavčič, 2008). In fact, when cell membrane electroporation / permeabilization increases, the conductivity increases, so the total current increases for constant applied voltage. Fig. 4A depicts the electric current difference between the value of I_{fin} (current reached at the end of the pulse, i.e. 100 μs after initial current increase) and I_{init} (current value at 10 μs after initial current increase, of arbitrary choice) normalized to the current value at the end of the pulse (ΔI_{norm}) for all the investigated specimens. In potato tissue, the permeabilization level was attained at applied voltage of amplitudes of about 100 V for both electrode configurations, needles and plates (Fig. 4 B,C), reaching a maximum permeabilization above 300 V. In apple tissue, when high-voltage pulses were delivered using 4-needle electrodes (Fig. 4B), the maximum increase of current during the pulse has been observed at permeabilizing applied voltage intensities of about 200 V, reaching a saturation level above 500 V. A slightly lower 'critical' electroporation value was found when the PEF treatment was delivered using plate electrodes (Fig. 4C), presenting the highest increase of current at 150 V (i.e. approx. 250 V/cm of the voltage-to-distance ratio). The animal tissue investigated displayed a constant level of current during the pulse at all the applied voltage amplitudes considered.

In addition, measured voltage and current waveforms, when parallel-plate electrode configuration was used, were analysed in terms of conductivity at 100th μs of the pulse (i.e. at the end of the first pulse) (Fig. 5). The conductivity was calculated according to Eq. (2).

$$\sigma = (I/U)(d/S) \quad (2)$$

where I/U is the ratio between current and voltage measured at 100 μs of the pulse, d is the distance between the electrodes, and S the contact surface between the electrode and the sample.

Fig. 5 displays the conductivity change at different applied voltage amplitudes (U). Raw data were fitted following a sigmoid curve (potato $R^2 = 0.90$; apple $R^2 = 0.83$; chicken $R^2 = 0.08$). It can be observed that the conductivity of plant tissues depends on the electric field magnitude. While in the potato specimen the conductivity slowly increases for U between 50 and 500 V, reaching a plateau at $U \geq 600$ V; in apple σ shows an abrupt increase between 100 and 200 V, and saturates at higher voltage amplitudes. Conversely, the conductivity of the chicken sample did not display any increase with increased voltage amplitude. The chicken was subjected to a different range of voltage amplitudes (i.e. between 200 V and 1000 V) than the one used for vegetable tissue (i.e. between 50 V and 1000 V), as the previously reported EIS data (Fig. 3D) clearly showed no changes in impedance for $U = 250$ V. Therefore, we

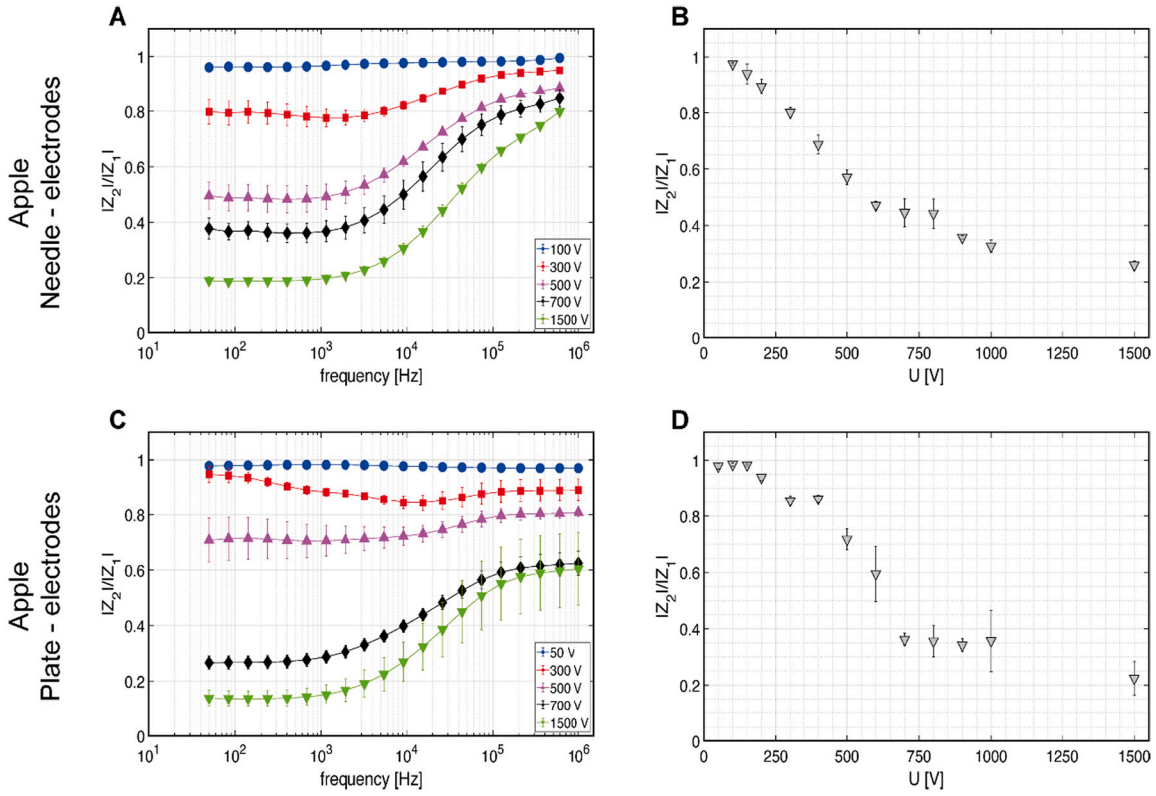

Fig. 2. Apple tissue normalized absolute impedance versus frequency at different applied voltage [U] amplitudes measured with 4-needle-electrodes (A), and plate-electrodes (C) configuration (not all the applied voltages are shown for clarity of presentation). Normalized absolute impedance at sampling frequency of 5 kHz versus the applied voltage [U] measured with 4-needle-electrodes (B), and plate-electrodes (D) configuration. Results are expressed as means ± standard deviations (error bars) of n = 4.

assumed that $U < 250$ V would not affect the tissue with the presented experimental set up.

3.3. *Electric field distributions and T_2 mapping in plant and animal tissues*

By means of MREIT we obtained electric field distributions in the potato, apple, and chicken samples when subjected to high-voltage electric pulses. For each biological sample considered, an optimal voltage amplitude was selected to obtain a good signal-to-noise ratio of MR signals (i.e. potato 750 V; apple 1180 V; chicken 860 V).

In addition to MREIT, T_2 mapping was also performed in the same samples to determine changes of tissue water content that would occur due to the application of electroporation pulses. In fact, T_2 relaxation value is correlated by the proton exchange between water and solutes and by diffusion of water protons through internally generated magnetic field gradients, causing magnetic susceptibility differences in the tissue exposed to the magnetic field, such as interfaces between air and liquid-filled pores. Therefore, T_2 values reflect – to a certain extent – the structure of the sample based on its water content (Defraeye et al., 2013). In our study, the effect of PEF treatment on T_2 relaxation times was evaluated in potato tuber, apple tissue and chicken skeletal muscle (Fig. 6) by measuring T_2 values before and after the application of the electroporation pulses. An area crossing the middle of the samples, with electrodes included, was taken into consideration as this area was exposed to a wide range of electric field values (solid lines in Fig. 6). In case of potato tuber, T_2 values obtained before application of high-voltage pulses (dotted line in Fig. 6A) revealed different water content in the tuber tissue's heterogeneous structure. After application of high-voltage pulses (dashed line in Fig. 6A), T_2 values decreased in areas exposed to the electric field strengths above approx. 250 V/cm, consistent with threshold value determined by EIS and current analysis. Interestingly, structures with a higher water content, i.e. with higher T_2 values, released more water after application of the pulses (measured as a larger decrease of T_2 values) compared to areas with a lower water content. The obtained trend of the T_2 decrease due to the application of high-voltage pulses is in accordance with the results obtained in the only comparable MR study on potato tuber (Kranjc et al., 2016), although that study did not take the pre-existing heterogenous distribution of water content within the tuber into consideration.

Apple exhibited less variation in T_2 values along the plane of observation compared to potato tuber. Slow decrease of T_2 values (dotted line in Fig. 6B) towards the edge of the apple sample suggests a higher water content in the centre of the sample. After the application of high-voltage pulses, we obtained a decrease of T_2 values (dashed line in Fig. 6B) in the middle of the apple and a slight increase of T_2 values towards the edge, presumably as a consequence of alteration of the tonoplast and the plasma membrane, causing a damaged compartmentalization that initiated diffusion of intracellular water towards extracellular spaces (Dellarosa et al., 2018, 2016). Due to limitation of the method, the apple tissue was exposed to higher applied voltage than potato, therefore we were not able to determine the electroporation threshold.

T_2 mapping of untreated and PEF-treated chicken breast fillets was also performed to understand if the applied PEF treatment could contribute to a change in the protein-water interaction and could lead to a loss of water from the sample. In our study, the application of PEF treatment did not induce any considerable change of the T_2 relaxation times (Fig. 6C).

4. Discussion

The aim of our study was to analyse the effect of PEF treatment by

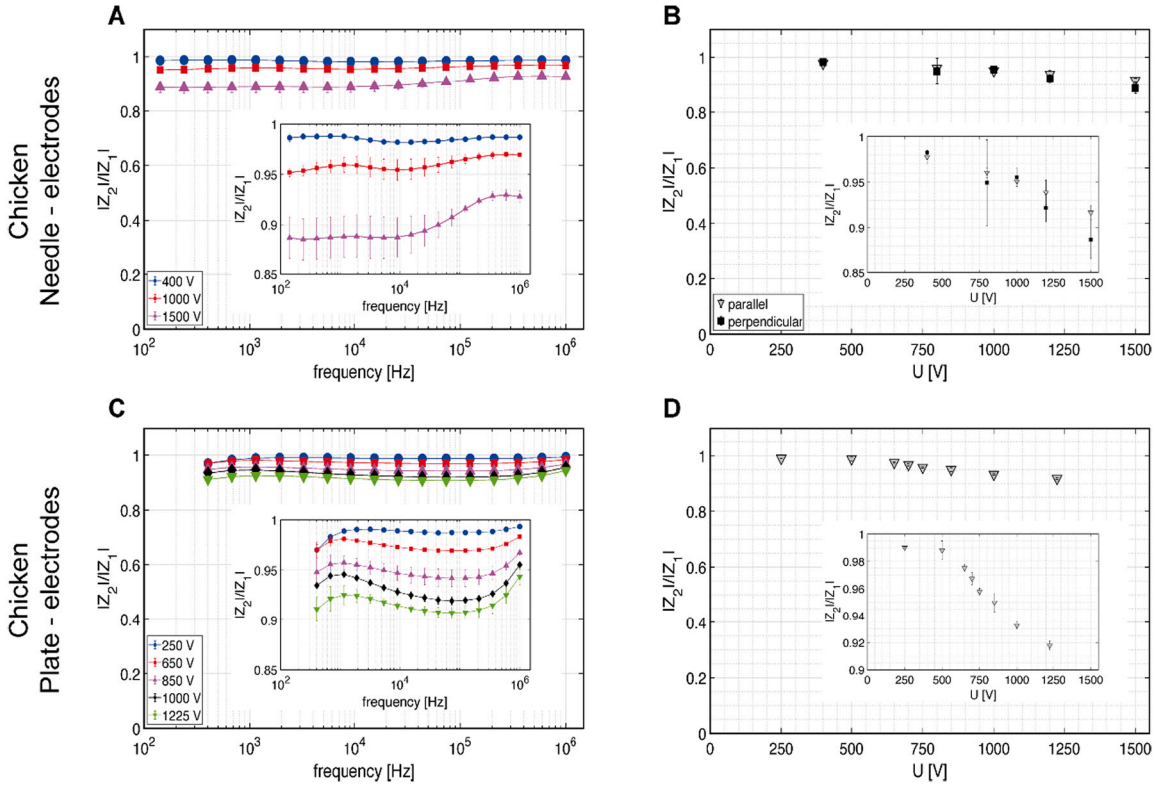

Fig. 3. Chicken breast muscle normalized absolute impedance versus frequency at different applied voltage [U] amplitudes measured with 4-needle-electrodes (A), and plate-electrodes (C) configuration (not all the applied voltages are shown for clarity of presentation). Normalized absolute impedance at sampling frequency of 5 kHz versus the applied voltage [U] measured with 4-needle-electrodes (B), and plate-electrodes (D) configuration. Measurements with 4-needle electrodes were performed applying high-voltage pulses parallelly or perpendicularly to the muscle fibre orientation. Results are expressed as means ± standard deviations (error bars) of n = 4.

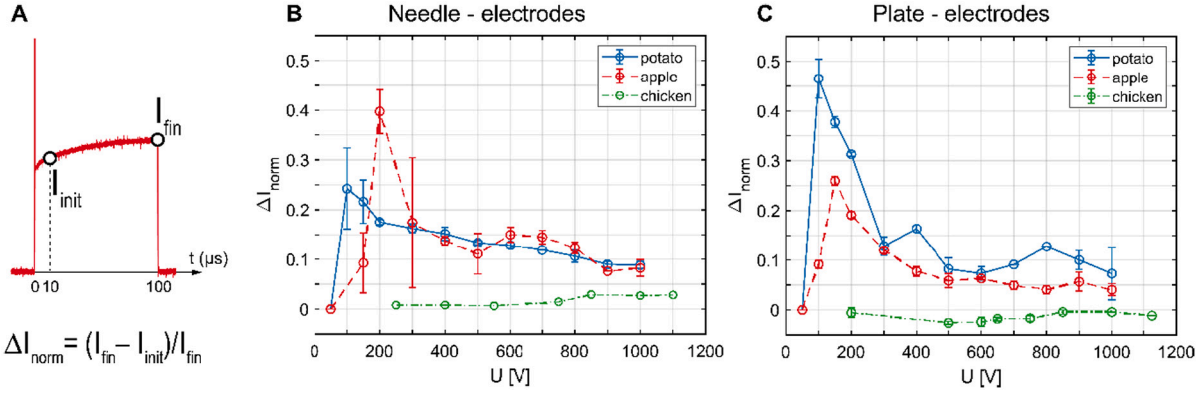

Fig. 4. Normalized electric current difference (ΔI_{norm}) between the final (I_{fin}) and initial (I_{init}) current values of the pulse portion with current increase following a decaying exponential function during the pulse (A). The difference was normalized to the current value at the end of the pulse (I_{fin}). An example of ΔI_{norm} obtained in potato, apple and chicken tissue exposed to electric pulses applied using needle (B) and plate (C) electrodes. U – applied voltage.

measuring electrical properties and water mobility in different raw biological materials of plant and animal origin, and to determine the level of membrane permeabilization due to electroporation.

Appropriate choice of methods used to test the cell membrane integrity in different multicellular systems could be of value in both food industry and research setting for determining and selecting adequate PEF treatment conditions and to monitor the lab- / industrial–scale processes. For successful application of the PEF treatment, it is important to understand that methods used to assess the degree of electroporation depend, among other, on highly inhomogeneous properties and complexity of food materials (Mahnič-Kalamiza et al., 2014), such as electrical properties, porosity, and structure. For this reason, the goal of our investigation was to explore the level of membrane permeabilization in diverse food materials (vegetables and meat), employing different methods used for the assessment of membrane permeabilization (i.e. EIS, current-voltage measurements, MRI, and T_2 mapping).

In general, the impedance of PEF-treated plant tissues (Figs. 1 and 2) shows a strong dependence on the magnitude of the applied voltage / electric field strength. Moreover, it can be observed that the analysed vegetables exhibit a non-linear decrease of their impedance modulus following the PEF treatment, suggesting the thresholding nature of the phenomenon (Figs. 1 and 2 B). The remarkable decrease of impedance

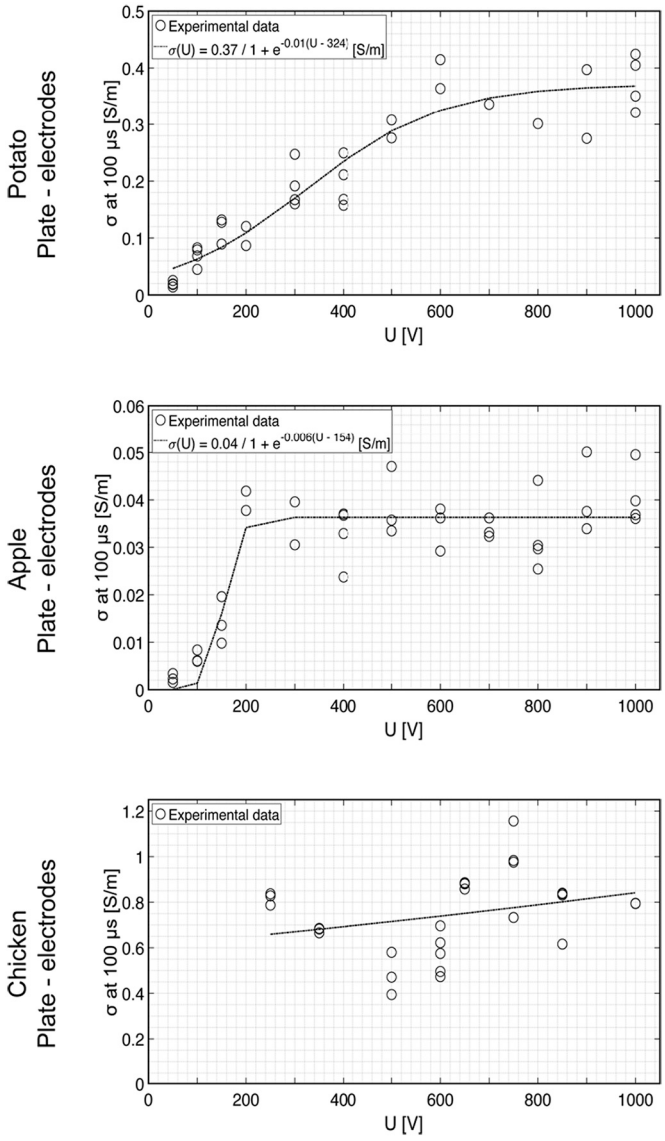

Fig. 5. Conductivity values at 100th µs of the first pulse recorded using plate electrodes configuration versus the amplitude of applied voltage [U], and the sigmoid function used to model the data.

can be explained by permeabilization of the cell membranes. In fact, since the cell membrane exhibits high impedance prior to the treatment, when electroporation occurs, it becomes more permeable, leading to a decrease of the said impedance (Ivorra, 2010). When analysing the impedance variation with different electrodes (needle and plate), the impedance decrease is reached at the same threshold levels. Thresholds, however, were found to be lower in potatoes than apples ($U \sim 150$ V; 250 V/cm for potatoes, $U \sim 300$ V; 500 V/cm for apples). The analysis of the current measured during the delivery of pulses can also be used as a simple method to detect changes in the dielectric properties of the tissue exposed to PEF treatment. When electroporation occurs, the cell membrane conductivity and permeability increase, which is reflected in the increase of the current during the pulse. As for the decrease in impedance, the maximum current increase was found to occur after a certain 'threshold' permeabilization level. The same as found by impedance analysis, the threshold as determined by current analysis was shown to be lower in potato than in apple ($U \sim 100$ V for potatoes, $U \sim 150$ V for apples) (Fig. 4). Observing the trend of measured conductivity at the end of the first pulse in plant tissues, reported in Fig. 5, a simple interpretation of these results would be that potato tissue is, from the water distribution perspective, much more homogeneous, and its conductivity increases almost linearly with the subsequent delivered electroporation pulses as more and more cells are electroporated since this renders a proportionally greater amount of extracellular liquid available for ionic transport (and thus current conduction). In the apple tissue, due to large amount of air in the tissue (i.e. higher porosity than potato) and dis-associated domains of tissue caused by pockets of air, higher field strength is necessary to cause a sufficient release of liquid. In fact, once a sufficiently conductive pathway in tissue is formed by a critical amount of released liquid, a step-like increase of conductivity is observed. Hence, different 'threshold' values of the magnitude of the applied voltage have been determined in relation to the different methods/plant tissues analysed in this study. The obtained results were not expected. For instance, since the apple cell size (≈ 130 µm diameter) is larger than that of potato (≈ 35 µm diameter), a lower electroporation threshold was expected in apple (i.e. the critical transmembrane potential is reached with external electric fields proportionally decreasing with the cell radius (Kotnik, Miklavčič, & Slivnik, 1998)). Similar observations were also previously reported in studies employing EIS for the evaluation of PEF-treatment efficacy in orange and potato tissues, where the latter, constituted of smaller size cells, was more efficiently electroporated when voltage-to-distance ratios (U/d) equal to 400 V/cm and 1000 V/cm were applied, respectively, employing two-plate electrodes (Ben Ammar, Lanoisellé, Lebovka, Van Hecke, & Vorobiev, 2011). The reported discrepancies could be explained by the dissimilar characteristics of the plant materials that could affect the electrical parameters, such as the electrical conductivity change (i.e. the ratio between the electrical conductivity of electroporated tissue and the electrical conductivity of intact tissue) (Ben Ammar et al., 2011); cell packing density; spatial distribution of air; overall tissue moisture; and initial cell turgor pressure. Moreover, plant cells are embedded in a matrix of cell walls, that can also affect passive electrical properties of biological systems. In fact, the charged groups of polysaccharides and other polymers that constitute the porous structure of cell walls contribute to the bulk

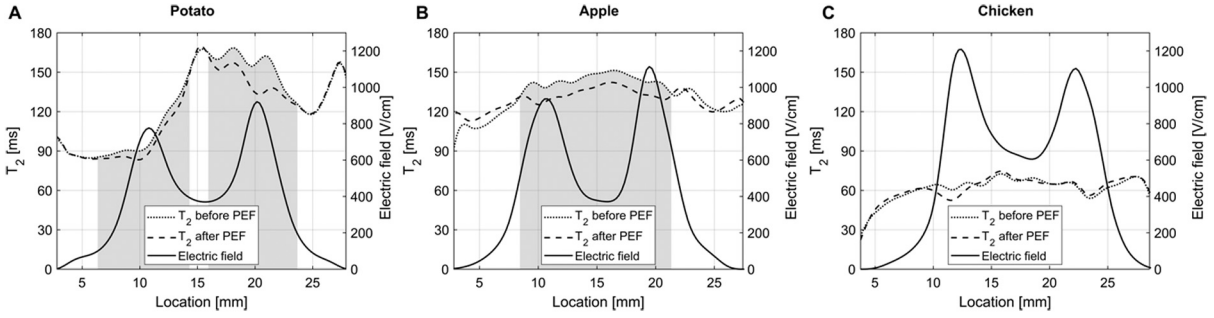

Fig. 6. T_2 – values acquired before (dotted lines) and after PEF treatment (dashed lines) in potato tuber (A), apple tissue (B), and chicken breast (C) along an area crossing the middle of the sample. Electric field (solid lines) was obtained by means of MREIT. Ranges of electric field corresponding to variations of T_2 value are marked by gray color background.

electrical properties of the tissue, and the change of ionic concentration in the extracellular media that may occur after electroporation (i.e. release of the cytoplasmatic fluid) could, in turn, induce changes in the measured electrical characteristics (Markx & Davey, 1999).

When chicken breast was analysed by applying the same train of 8 high-voltage pulses, we did not observe changes in its electrical properties as we did in plant tissue. In fact, only a small (but progressive with the increase of the applied voltage) decrease of the absolute impedance was shown (Fig. 3), which could be ascribed to a slight heating of the tissue subjected to electric pulses. Changes in current/conductivity observed (Figs. 4 and 5) were negligible. Similar ex vivo experiments have previously been conducted on chicken and beef liver (Kranjc, Bajd, Sersa, Woo, & Miklavcic, 2012; Langus et al., 2016) where, contrary to observations in the present study, an exponential increase in current amplitude has been shown when applying the same train of pulses. The discrepancies found, although surprising, can be explained by the different anatomy of chicken breast vs. beef liver, the latter being constituted of hepatocytes that are not affected by *post-mortem* degradation processes typical of muscle fibres (Zaefarian, Abdollahi, Cowieson, & Ravindran, 2019).

The electroporation assessment methodologies we used in this study are largely associated not only with the degree of cell permeabilization, but with other secondary effects. For instance, some of the consequences of membrane permeabilization correspond to structure modifications and intracellular fluid leaking outside the cell (Puértolas, Luengo, Álvarez, & Raso, 2012). The latter could play an important role in affecting the measured electrical properties of plant cells, characterised by high gradient of osmotic pressure between the intra- and extracellular fluids. On the other hand, *post-mortem* skeletal muscle undergoes a series of physical and biochemical modifications related to myofibrillar structure, cytoskeleton, and membranes (Schreurs & Uijttenboogaart, 2000). Soon after the onset of rigour, plasma membrane and the membrane of the sarcoplasmic reticulum degenerate from their normal laminar structure, increasing their degree of porosity (Damez, Clerjon, Abouelkaram, & Lepetit, 2008). *Rigor mortis* onset in poultry is more rapid than in bovine and porcine muscles since, chicken breast in particular, is mainly composed of fast-twitching fibres that are associated with the anaerobic glycolysis (Schreurs & Uijttenboogaart, 2000). As rigour progresses, the space for water to be held in the myofibrils is reduced, and fluid can be forced into the extra-myofibrillar spaces, where it is more easily lost as drip (Huff-Lonergan & Lonergan, 2005). Therefore, it is quite possible that, at the time we performed treatment and analysis (ca. 48 h *post-mortem*), the muscle fibre membranes were already significantly degraded (Schreurs & Uijttenboogaart, 2000), and so no further changes in the electrical properties were detected following the PEF treatment.

To confirm this hypothesis, our experimental design included the characterization of the food tissue response in terms of water mobility to different levels of electric field strength by the MRI technique. By employing T_2 relaxometry measurements, it is possible to obtain information related to the water content and the interaction of water with the surrounding macromolecules. Electroporation pulses can induce structural changes, such as the cell membrane damage, affecting NMR relaxation rates. In fact, the primary effect of PEF treatment is related to cell membrane electroporation and to a consequential release of the intracellular content. We observed a general decrease of T_2 in plant tissues (Fig. 6 A,B) that can be ascribed to the loss of compartmentalization and diffusion of intracellular water and ion leakage through the tonoplast and the plasmalemma membranes, resulting in inner morphology modifications (e.g. overall volume shrinkage) and in different water-solutes interactions, as already reported previously (Dellarosa et al., 2018; Hills & Remigereau, 1997; Kranjc et al., 2016). In our study, we also observed that potato specimens exhibit a larger variation of T_2 relaxation rates compared to apple, which could conceivably be attributed to a more extensive (re)distribution of intracellular fluids. This could explain the lower electroporation 'threshold' we detected in potato tissue (as compared to apple) when measuring the electrical properties. Moreover, the extent of T_2 changes in PEF-treated potato and apple parenchyma we observed are comparable to those already reported in literature (Dellarosa et al., 2018; Kranjc et al., 2016). On the contrary, we were unable to detect changes in bulk water mobility in chicken breast muscles under the present experimental conditions by means of the MR imaging. Similar observations were previously reported in PEF-treated post rigour beef muscle (72 h *post-mortem*, electric field applied 1.9 kV/cm), where no major changes of the T_2 relaxation times were observed, suggesting that the PEF treatment did not induce any modification of the muscle fibre membranes, while a significant weight loss was due to the fluid in the extracellular space (O'Dowd, Arimi, Noci, Cronin, & Lyng, 2013).

5. Conclusions

In our study, the application of PEF treatments to different matrices of food interest (plant tissues and skeletal muscles) was experimentally investigated, and the level of membrane permeabilization due to electroporation was explored by means of various PEF assessing methodologies. Electrical properties measurements were performed comparing two different electrode configurations, a 4-electrode system with needles inserted in the tissues, and a plate-electrode system in contact with the surface of samples. In the plant tissues considered (potatoes and apples) we demonstrated that data recorded before and after the high-voltage pulses are significantly influenced not only by the structural characteristics of biological tissues (e.g. cell size), but that the exchange of fluids between intra- and extra-cellular environments dramatically influences the electrical properties. The same effect was observed analysing the conductivity change by monitoring current waveforms. Nevertheless, skeletal muscle used in this study did not yield similar results, which demonstrates that the aforementioned electroporation assessment methods must be used critically and with caution for PEF treatment optimization. Magnetic resonance electrical impedance tomography for monitoring the electric field distribution and T_2 mapping confirmed that the plant cell membranes' breakdown due to electroporation caused a significant decrease of T_2 relaxation times, most probably due to the release of intracellular content into the extracellular space. On the contrary, the muscle fibres seemed to be unaffected by the PEF treatment. We assume this is a consequence of alteration of sarcoplasmic membranes caused by *post-mortem* biodegradative processes. The findings of this research can be of support in the future selection of meat conditions (i.e. aging time) for the effectiveness of PEF treatment applications. This work provides important insights and calls for critical choice of electroporation assessment methods, also with respect to matrix characteristics (e.g. physiological state) in determination of PEF treatment conditions.

Conflict of interest and authorship conformation

All authors have participated in drafting the article or revising it critically for important intellectual content and have approved the final version. Details on authors' individual contributions are found in the separate Author statement document.

This manuscript has not been submitted to, nor is under review at, another journal or other publishing venue.

The authors have no affiliation with any organization with a direct or indirect financial interest in the subject matter discussed in the manuscript.

Acknowledgements

The author JG would like to gratefully acknowledge the financial support provided by *Marco Polo Mobility Programme* funded by Department of Agricultural and Food Sciences of University of Bologna to conduct the presented study at University of Ljubljana.

The authors MK, SMK and DM would like to acknowledge the financial support through research programs and projects granted by the Slovenian Research Agency (ARRS), namely the research programme P2-0249, and the postdoctoral project Z7-1886 (awarded to SMK) and research project J2-1733 (awarded to MK). This study was conducted within the Infrastructure Programme: Network of research infrastructure centres at the University of Ljubljana (MRIC UL IP-0510), also funded by the Slovenian Research Agency (ARRS).

The authors also acknowledge Amadori Company (San Vittore di Cesena, Italy) for providing chicken muscle samples.

References

Angersbach, A., Heinz, V., & Knorr, D. (1999). Electrophysiological model of intact and processed plant tissues: Cell disintegration criteria. *Biotechnology Progress*. https://doi.org/10.1021/bp990079f

Angersbach, A., Heinz, V., & Knorr, D. (2002). Evaluation of process-induced dimensional changes in the membrane structure of biological cells using impedance measurement. *Biotechnology Progress*. https://doi.org/10.1021/bp020047j

Ben Ammar, J., Lanoisellé, J. L., Lebovka, N. I., Van Hecke, E., & Vorobiev, E. (2011). Impact of a pulsed electric field on damage of plant tissues: Effects of cell size and tissue electrical conductivity. *Journal of Food Science*. https://doi.org/10.1111/j.1750-3841.2010.01893.x

Bhat, Z. F., Morton, J. D., Mason, S. L., & Bekhit, A. E.-D. A. (2019). Current and future prospects for the use of pulsed electric field in the meat industry. *Critical Reviews in Food Science and Nutrition, 59*, 1660–1674. https://doi.org/10.1080/10408398.2018.1425825

Carr, H. Y., & Purcell, E. M. (1954). Effects of diffusion on free precession in nuclear magnetic resonance experiments. *Physics Review, 94*, 630–638. https://doi.org/10.1103/PhysRev.94.630

Castellví, Q., Mercadal, B., & Ivorra, A. (2017). Assessment of electroporation by electrical impedance methods. In *Handbook of electroporation*. https://doi.org/10.1007/978-3-319-32886-7_164

Chalermchat, Y., Malangone, L., & Dejmek, P. (2010). Electropermeabilization of apple tissue: Effect of cell size, cell size distribution and cell orientation. *Biosystems Engineering, 105*, 357–366. https://doi.org/10.1016/J.BIOSYSTEMSENG.2009.12.006

Cukjati, D., Batiuskaite, D., André, F., Miklavčič, D., & Mir, L. M. (2007). Real time electroporation control for accurate and safe in vivo non-viral gene therapy. *Bioelectrochemistry.*. https://doi.org/10.1016/j.bioelechem.2006.11.001

Damez, J. L., Clerjon, S., Abouelkaram, S., & Lepetit, J. (2008). Electrical impedance probing of the muscle food anisotropy for meat ageing control. *Food Control, 19*, 931–939. https://doi.org/10.1016/j.foodcont.2007.09.005

Defraeye, T., Lehmann, V., Gross, D., Holat, C., Herremans, E., Verboven, P., … Nicolai, B. M. (2013). Application of MRI for tissue characterisation of "Braeburn" apple. *Postharvest Biology and Technology, 75*, 96–105. https://doi.org/10.1016/j.postharvbio.2012.08.009

Dellarosa, N., Laghi, L., Ragni, L., Dalla Rosa, M., Galante, A., Ranieri, B., Florio, T. M., & Alecci, M. (2018). Pulsed electric fields processing of apple tissue: Spatial distribution of electroporation by means of magnetic resonance imaging and computer vision system. *Innovative Food Science and Emerging Technologies*. https://doi.org/10.1016/j.ifset.2018.02.010

Dellarosa, N., Ragni, L., Laghi, L., Tylewicz, U., Rocculi, P., & Dalla Rosa, M. (2016). Time domain nuclear magnetic resonance to monitor mass transfer mechanisms in apple tissue promoted by osmotic dehydration combined with pulsed electric fields. *Innovative Food Science and Emerging Technologies, 37*, 345–351. https://doi.org/10.1016/j.ifset.2016.01.009

Golberg, A., Sack, M., Teissie, J., Pataro, G., Pliquett, U., Saulis, G., … Frey, W. (2016). Energy-efficient biomass processing with pulsed electric fields for bioeconomy and sustainable development. *Biotechnology for Biofuels*. https://doi.org/10.1186/s13068-016-0508-z

Grimnes, S., Martinsen, Ø. G., Grimnes, S., & Martinsen, Ø. G. (2015). Chapter 3 – Dielectrics. In *Bioimpedance and bioelectricity basics*. https://doi.org/10.1016/B978-0-12-411470-8.00003-9

Hills, B. P., & Remigereau, B. (1997). NMR studies of changes in subcellular water compartmentation in parenchyma apple tissue during drying and freezing. *International Journal of Food Science and Technology*. https://doi.org/10.1046/j.1365-2621.1997.00381.x

Hjouj, M., & Rubinsky, B. (2010). Magnetic resonance imaging characteristics of nonthermal irreversible electroporation in vegetable tissue. *The Journal of Membrane Biology, 236*. https://doi.org/10.1007/s00232-010-9281-2

Huff-Lonergan, E., & Lonergan, S. M. (2005). Mechanisms of water-holding capacity of meat: The role of postmortem biochemical and structural changes. *Meat Science*. https://doi.org/10.1016/j.meatsci.2005.04.022

Ivorra, A. (2010). *Tissue electroporation as a bioelectric phenomenon: Basic concepts* (pp. 23–61). Berlin, Heidelberg: Springer. https://doi.org/10.1007/978-3-642-05420-4_2

Joy, M., Scott, G., & Henkelman, M. (1989). In vivo detection of applied electric currents by magnetic resonance imaging. *Magnetic Resonance Imaging, 7*. https://doi.org/10.1016/0730-725X(89)90328-7

Khang, H. S., Lee, B. I., Oh, S. H., Woo, E. J., Lee, S. Y., Cho, M. H., … Seo, J. K. (2002). J-substitution algorithm in magnetic resonance electrical impedance tomography (MREIT): Phantom experiments for static resistivity images. *IEEE Transactions on Medical Imaging, 21*. https://doi.org/10.1109/TMI.2002.800604

Kotnik, T., Miklavčič, D., & Slivnik, T. (1998). Time course of transmembrane voltage induced by time-varying electric fields - a method for theoretical analysis and its application. *Bioelectrochemistry and Bioenergetics, 45*, 3–16. https://doi.org/10.1016/S0302-4598(97)00093-7

Kotnik, T., Rems, L., Tarek, M., & Miklavcic, D. (2019). Membrane electroporation and electropermeabilization: Mechanisms and models. *Annual Review of Biophysics*. https://doi.org/10.1146/annurev-biophys-052118-115451

Kranjc, M., Bajd, F., Serša, I., de Boevere, M., & Miklavčič, D. (2016). Electric field distribution in relation to cell membrane electroporation in potato tuber tissue studied by magnetic resonance techniques. *Innovative Food Science and Emerging Technologies*. https://doi.org/10.1016/j.ifset.2016.03.002

Kranjc, M., Bajd, F., Sersa, I., Woo, E. J., & Miklavcic, D. (2012). Ex vivo and in silico feasibility study of monitoring electric field distribution in tissue during electroporation based treatments. *PLoS One*. https://doi.org/10.1371/journal.pone.0045737

Langus, J., Kranjc, M., Kos, B., Šuštar, T., & Miklavčič, D. (2016). Dynamic finite-element model for efficient modelling of electric currents in electroporated tissue. *Scientific Reports, 6*. https://doi.org/10.1038/srep26409

Lebovka, N., & Vorobiev, E. (2017). Techniques to detect electroporation in food tissues. In *Handbook of electroporation*. https://doi.org/10.1007/978-3-319-32886-7_150

Lv, Y., Cheng, X., Chen, S., Liu, H., Wang, Y., Yao, C., & Rubinsky, B. (2020). Analysis of the electric field-dependent current during electroporation pulses. *IEEE Access, 8*, 93850–93856. https://doi.org/10.1109/ACCESS.2020.2995151

Mahnič-Kalamiza, S., Miklavčič, D., & Vorobiev, E. (2015). Dual-porosity model of mass transport in electroporated biological tissue: Simulations and experimental work for model validation. *Innovative Food Science and Emerging Technologies*. https://doi.org/10.1016/j.ifset.2014.09.011

Mahnič-Kalamiza, S., Vorobiev, E., & Miklavčič, D. (2014). Electroporation in food processing and biorefinery. *The Journal of Membrane Biology, 247*, 1279–1304. https://doi.org/10.1007/s00232-014-9737-x

Markx, G. H., & Davey, C. L. (1999). The dielectric properties of biological cells at radiofrequencies: Applications in biotechnology. *Enzyme and Microbial Technology*. https://doi.org/10.1016/S0141-0229(99)00008-3

Novickij, V., Grainys, A., Butkus, P., Tolvaišienė, S., Švedienė, J., Paškevičius, A., & Novickij, J. (2016). High-frequency submicrosecond electroporator. *Biotechnology and Biotechnological Equipment*. https://doi.org/10.1080/13102818.2016.1150792

O'Dowd, L. P., Arimi, J. M., Noci, F., Cronin, D. A., & Lyng, J. G. (2013). An assessment of the effect of pulsed electrical fields on tenderness and selected quality attributes of post rigour beef muscle. *Meat Science, 93*, 303–309. https://doi.org/10.1016/j.meatsci.2012.09.010

Pavlin, M., Kandušer, M., Reberšek, M., Pucihar, G., Hart, F. X., Magjarević, R., & Miklavčič, D. (2005). Effect of cell electroporation on the conductivity of a cell suspension. *Biophysical Journal, 88*. https://doi.org/10.1529/biophysj.104.048975

Pavlin, M., & Miklavčič, D. (2008). Theoretical and experimental analysis of conductivity, ion diffusion and molecular transport during cell electroporation - relation between short-lived and long-lived pores. *Bioelectrochemistry.*. https://doi.org/10.1016/j.bioelechem.2008.04.016

Puértolas, E., Luengo, E., Álvarez, I., & Raso, J. (2012). Improving mass transfer to soften tissues by pulsed electric fields: Fundamentals and applications. *Annual Review of Food Science and Technology*. https://doi.org/10.1146/annurev-food-022811-101208

Schreurs, F. J. G., & Uijttenboogaart, T. G. (2000). Post-mortem changes in chicken muscle. *World's Poultry Science Journal, 56*. https://doi.org/10.1079/wps20000023

Serša, I. (2008). Auxiliary phase encoding in multi spin-echo sequences: Application to rapid current density imaging. *Journal of Magnetic Resonance*. https://doi.org/10.1016/j.jmr.2007.10.009

Verdiglione, R., & Cassandro, M. (2013). Characterization of muscle fiber type in the pectoralis major muscle of slow-growing local and commercial chicken strains. *Poultry Science, 92*, 2433–2437. https://doi.org/10.3382/ps.2013-03013

Zaefarian, F., Abdollahi, M. R., Cowieson, A., & Ravindran, V. (2019). Avian liver: The forgotten organ. *Animals, 9*. https://doi.org/10.3390/ani9020063